Electrochemically Induced Deformation Determines the Rate of Lithium Intercalation in Bulk TiS2

Simon Fleischmann, Hui Shao, Pierre-Louis Taberna, Patrick Rozier, Patrice Simon

ACS Energy LETTERS

http://pubs.acs.org/journal/aelccp

Electrochemically Induced Deformation Determines the Rate of Lithium Intercalation in Bulk TiS_2

Simon Fleischmann,* Hui Shao, Pierre-Louis Taberna, Patrick Rozier, and Patrice Simon

Cite This: *ACS Energy Lett.* 2021, 6, 4173–4178

Read Online

ACCESS | Metrics & More | Article Recommendations | Supporting Information

ABSTRACT: Understanding the kinetic limitations of intercalation reactions is essential to create high-power intercalation host materials. In this Letter, we show the existence of both diffusion-limited and non-diffusion-limited lithiation regimes in the model material bulk TiS_2. The regions can be clearly identified by electrochemical impedance spectroscopy. A decreasing charge-transfer resistance is observed with increasing electrode polarization in the diffusion-limited region, whereas it remains constant when the electrochemical process is non-diffusion-limited. We highlight how TiS_2 interlayer deformation is closely tied to the intercalation kinetics. While regions of TiS_2 interlayer expansion/contraction are correlated with diffusion limitations, lithiation occurring under constant interlayer spacing is non-diffusion-limited: the material exhibits pseudocapacitive behavior. Larger TiS_2 interlayer spacing results in faster ionic transport. The study sheds light on the close ties between deformation, interlayer distance, and intercalation kinetics in a model layered host material.

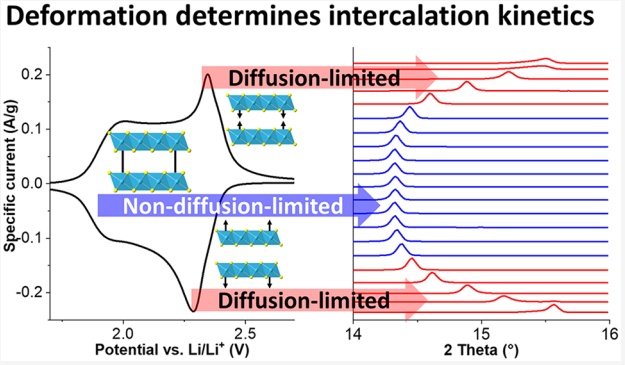

Electrochemical intercalation of ions into host electrode materials is the basis of applications ranging from electrochemical energy storage[1−3] to water desalination[4,5] and element recovery.[6] To accommodate the strain induced by the intercalated ions, host materials often undergo first-order phase transformations, such as the staging mechanism in graphite[7,8] or two-phase reactions of lithium iron phosphate ($LiFePO_4$–$FePO_4$)[9,10] and spinel lithium titanate ($Li_4Ti_5O_{12}$–$Li_7Ti_5O_{12}$)[11] during lithium intercalation.

In some host materials, guest ions can electrochemically intercalate via a solid-solution reaction mechanism, often causing lattice strains but no first-order phase transformations. In the case of titanium disulfide (TiS_2)—which was the first lithium intercalation host described by Whittingham in 1976—the electrochemical intercalation of lithium occurs via a continuous variation of the composition x in Li_xTiS_2 according to[1,12]

$$x\mathrm{Li}^+ + x\mathrm{e}^- + \mathrm{TiS}_2 \rightarrow \mathrm{Li}_x\mathrm{TiS}_2, \quad 0 \leq x \leq 1 \qquad (1)$$

Conway described this Faradaic intercalation reaction as a two-dimensional electrosorption process that could be modeled with a Langmuir-type adsorption isotherm, with the electrode potential varying as a function of the Li^+ lattice occupancy x.[13] This sloping sigmoidal potential curve is notably different from intercalation reactions involving first-order phase transformations that result in potential plateaus during galvanostatic charge/discharge cycles.

Faradaic intercalation reactions via the solid-solution mechanism can occur with mirror-image cyclic voltammograms (CVs), i.e., with negligible potential hysteresis between the cathodic and anodic processes and with kinetics not limited by solid-state ion diffusion over a wide potential range.[14] This behavior was observed, among others, in the $Li_xNb_2O_5$ system and labeled as pseudocapacitive intercalation due to the similarity of potential development and kinetics to capacitive processes.[14,15] It can also be found in nanostructured materials, where diffusion paths are drastically reduced and reaction site energies may become dispersed.[14,16,17] Muller et al. studied the lithiation of few-layered, nanocrystalline TiS_2, where both structural distortions and diffusion paths are drastically reduced compared to those of the corresponding bulk material.[18] Cook

Received: September 8, 2021
Accepted: October 6, 2021
Published: November 1, 2021

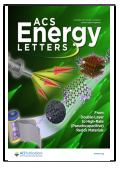

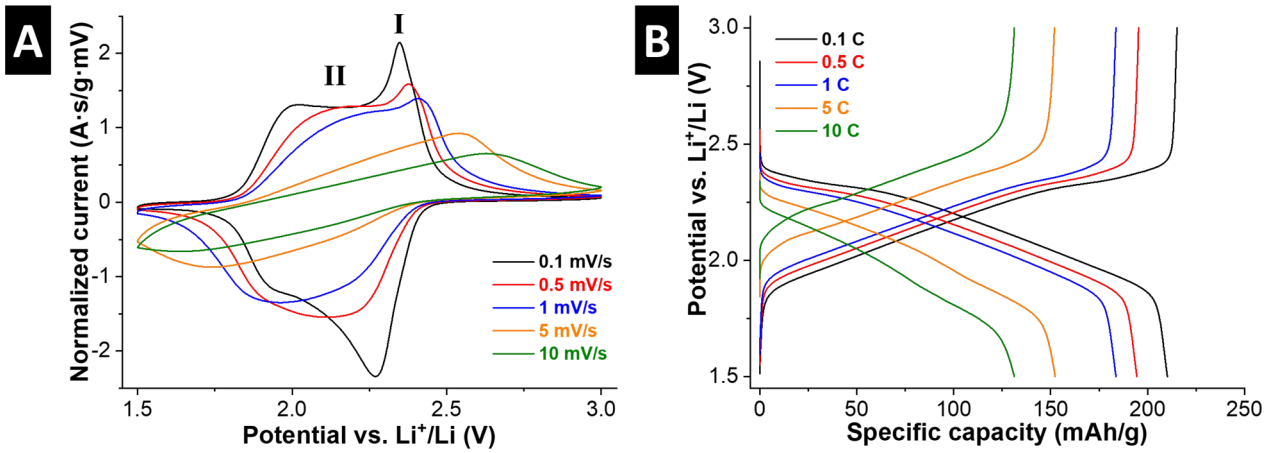

Figure 1. Electrochemical characterization of bulk TiS_2 in coin cells versus lithium metal in LP30 electrolyte. (A) Normalized cyclic voltammograms with sweep rates between 0.1 and 10 mV/s. The redox peak region is marked as I, and the rectangular current region is marked as II. (B) Galvanostatic charge/discharge cycles with rates between 0.1 and 10 C (23.9−2390 mA/g).

et al. demonstrated the emergence of pseudocapacitive lithium intercalation in the closely related layered material MoS_2 when first-order phase transitions were suppressed as a consequence of nanostructuring.[19] While these studies identified pseudocapacitive lithium intercalation properties in the nanostructured form of the host materials, it remains unclear how lattice distortion during solid-solution intercalation reactions affects the ionic transport in bulk host materials and therefore the intrinsic electrochemical properties of the systems.

It was found that the reduction of volume changes can lead to fast kinetics for lithium intercalation in the niobium−tungsten oxide system[20] and for proton intercalation in the $WO_3{\cdot}xH_2O$ system[21] (for both solid-solution and two-phase type reactions). A recent perspective by Augustyn et al. discussed the close links between the kinetics of electrochemical intercalation reactions and the deformation response of the host materials and stressed the need for in situ and operando methods to closely investigate the underlying electro-chemo-mechanical properties of intercalation hosts.[22]

In this work, we investigate the relationship between deformation and lithium intercalation kinetics in bulk TiS_2, a model layered host material for solid-solution lithium intercalation. We highlight how TiS_2 interlayer expansion/contraction is closely tied to the intercalation kinetics. Using galvanostatic intermittent titration technique (GITT), in situ X-ray diffraction (XRD), and electrochemical impedance spectroscopy (EIS), we show two distinct kinetic regimes of diffusion-limited and non-diffusion-limited (pseudocapacitive) lithium intercalation. We further demonstrate how lithium transport kinetics are increased by an expanded TiS_2 interlayer distance. The findings clearly illustrate the close ties between deformation, interlayer distance, and intercalation kinetics experimentally, giving guidance for the design of future high-power ion intercalation hosts and providing experimental tools to analyze their electrochemical properties.

Commercial TiS_2 powder with a flake-like morphology (mesh 200, lateral particle size up to ca. 50 μm, Figure S1, specific surface area (BET)[23] ca. 7 m^2/g, Figure S2A) was used in this work to study the intrinsic electrochemical Li^+ intercalation properties of bulk TiS_2. According to XRD analysis, the material exhibits an interlayer distance (c-lattice parameter) of 0.569 nm (Figure S2B), consistent with the structure of trigonal 1T-TiS_2 (space group $P\bar{3}m1$).[24]

The electrochemical properties of bulk TiS_2 were evaluated by CV (Figure 1A) and galvanostatic charge/discharge experiments (Figure 1B) in lithium-containing organic electrolyte (LP30). From the CV at the lowest sweep rate of 0.1 mV/s, the onset of a sharp cathodic redox peak can be detected at around 2.4 V vs Li^+/Li (region I in Figure 1A). Following the redox peak, at lower potentials between ca. 2.2 and 1.9 V vs Li^+/Li, a broad cathodic current feature with a rectangular shape is observed (region II in Figure 1B). In the anodic scan, the same features are exhibited in an almost mirror-image to the cathodic step at the lowest sweep rate; however, at increased rates, especially of 5 mV/s and more, peak broadening and increased overpotentials prevent a clear separation of the two current features. From the galvanostatic tests, equivalent observations can be made. Two regions can be identified, with a relatively flat potential plateau between ca. 2.4 and 2.25 V vs Li^+/Li, followed by a sloping region down to about 1.9 V vs Li^+/Li.

The Li^+ intercalation reaction in bulk TiS_2 was previously described as a solid-solution process with a variable phase composition of Li_xTiS_2 (with $x \leq 1$);[1,12,13,25] however, CV and galvanostatic cycling strongly point to the existence of two distinguishable regions, I and II, with different electrochemical signatures. The underlying mechanisms leading to two distinguishable kinetic regimes in bulk TiS_2 remain unclear and will thus be analyzed in the following.

In the CVs, the normalized redox peak current decreases with higher sweep rates, while the normalized rectangular current region stays relatively constant up to a sweep rate of about 1 mV/s. This implies different kinetic properties of the two regions, with the redox peak region appearing diffusion-limited and the rectangular current region appearing non-diffusion-limited. The so-called b-value analysis[14,26] can serve as a first guidance to study the kinetic limitations of electrochemical processes. Plotting the logarithmic peak current versus the logarithmic sweep rate at different rates (Figure 2B), the slope of the fitting line will vary between 0.5 (ideally diffusion-limited process) and 1.0 (ideally surface-limited process). Our analysis shows a trend to a semi-infinite diffusion limitation of the peak region (b = 0.72), while the reaction kinetics in the rectangular region trend toward a more non-diffusion-limited behavior (b = 0.88) within the sweep rates of 0.1−1 mV/s.[14] It should be noted that relatively slow sweep rates were used for this analysis owing to the high distortion of the CVs at higher rates which

https://doi.org/10.1021/acsenergylett.1c01934
ACS Energy Lett. 2021, 6, 4173−4178

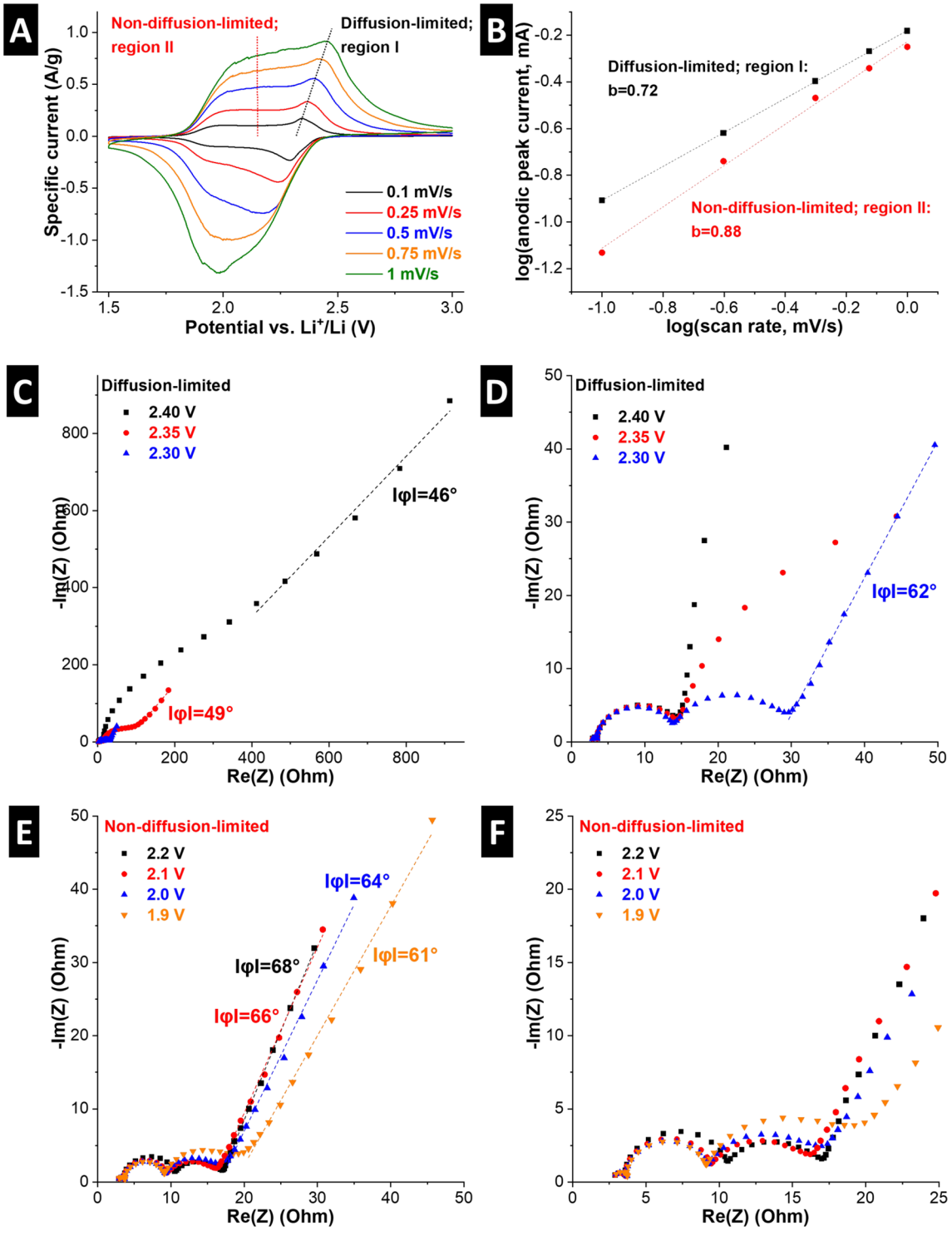

Figure 2. Analysis of the Li^+ intercalation process in bulk TiS_2 in LP30 electrolyte in a three-electrode setup. (A) Cyclic voltammograms with sweep rates between 0.1 and 1 mV/s. (B) Kinetic study using *b*-value analysis, comparing the dependence of the peak current from the sweep rate at the redox peak with shifting peak potential (region I) and at the current measured at 2.15 V vs Li^+/Li for the rectangular, potential-independent feature (region II). Electrochemical impedance spectra measured at different potentials (C, and zoomed-in, D) around the redox peak potential (region I, diffusion-limited process) and (E, and zoomed-in, F) around the region of potential-independent current (region II, non-diffusion-limited process). Phase angles φ are calculated from the slope of the fitting line in the Warburg-like region.

result from ohmic limitations and the very large particle sizes with long diffusion paths. A control experiment with a different electrolyte solvent (acetonitrile, Figure S3) shows similar results (b = 0.70 for the diffusion-limited region I and b = 0.95 for the non-diffusion-limited region II).

In our case, it is clear that the *b*-values found with this analysis method give only some trends regarding the kinetics of the electrochemical processes, in part due to the highly distorted CVs at increased sweep rates, leading to strong shifts of the redox potentials. Therefore, we utilized electrochemical

https://doi.org/10.1021/acsenergylett.1c01934
ACS Energy Lett. 2021, 6, 4173−4178

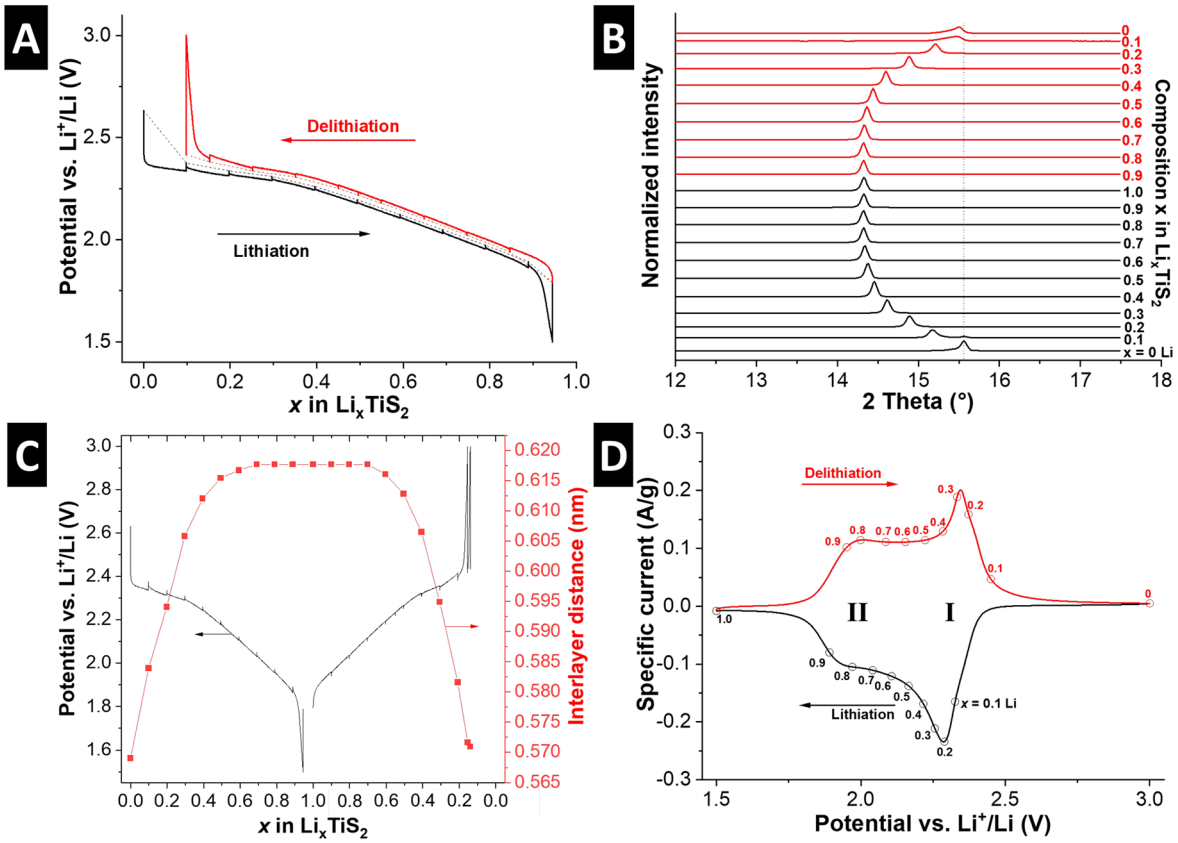

Figure 3. Electrochemical in situ XRD experiment of Li^+ intercalation in bulk TiS_2 in LP30 electrolyte. (A) Potential curve via galvanostatic intermittent titration technique (GITT) of TiS_2 during (de)lithiation in an in situ cell. (B) XRD patterns recorded after a charge equivalent to 0.1 e^- per TiS_2 (corresponding to 0.1 Li^+ intercalated) was passed, and (C) the corresponding TiS_2 interlayer distance as a function of electrode potential and composition. (D) CV at 0.1 mV/s taken from a coin cell with markers highlighting the composition x of Li_xTiS_2 based on the integrated charge.

impedance spectroscopy (EIS) to deconvolute the processes. The EIS plots in the 2.4−2.3 V vs Li^+/Li potential range (region I, Figure 2C) show a high-frequency loop that does not change with the applied potential, associated with the current collector/TiS_2 film interfacial resistance. The EIS of the TiS_2 film shows the expected blocking electrode behavior at 3 V vs Li^+/Li, with a sharp increase of the impedance at low frequencies (Figure S4A). Upon lithiation (from 2.4 V down to 2.3 V vs Li^+/Li), the middle-frequency loop in Figure 2C,D is associated with the charge-transfer resistance that decreases with increased electrode polarization, while the low-frequency part shows a Warburg-type process for 2.4 and 2.35 V vs Li^+/Li (see also Figure 3C and Figure S4B), in agreement with a diffusion-limited process (phase angle $|\varphi| \approx 45°$). At 2.3 V vs Li^+/Li, the low-frequency angle $|\varphi| = 62°$, as this potential lies in the transition zone between the diffusion-limited and the non-diffusion-limited processes. Figure 2E,F shows the EIS plots in the 2.2−1.9 V vs Li^+/Li potential range (region II). In this region, the charge-transfer resistance is smaller than in the transition region at 2.3 V vs Li^+/Li, and it stays constant over the entire potential range of the non-diffusion-limited lithiation regime. Together with the phase angle φ ($68° > |\varphi| > 61°$), this supports the existence of fast charge-transfer kinetics, in agreement with the rectangular current feature and Conway's description of specific Li^+ adsorption in the interlayer of bulk TiS_2, i.e., pseudocapacitive Li^+ intercalation. Our analysis demonstrates the utility of EIS to identify pseudocapacitive processes, comparable to the 3D Bode analysis described by Ko et al.[27,28]

To understand why the solid-solution intercalation reaction of lithium into TiS_2 occurs not in a continuous manner but in two different kinetic regimes, the crystallographic changes of Li_xTiS_2 are analyzed as a function of the composition x during electrochemical cycling via in situ XRD. Previous in situ XRD experiments indicated a progressive variation of the bulk TiS_2 interlayer spacing (c-parameter) up to a potential of about 1.5 V vs Li^+/Li,[18] indicative of a continuous solid-solution intercalation process. However, these experiments were carried out under dynamic conditions[18] and thus remain inconclusive as to the fundamental mechanisms governing the electrochemical lithiation process of bulk TiS_2. Therefore, we examine the crystallographic changes during electrochemical (de)lithiation under quasi-equilibrium conditions by utilizing galvanostatic intermittent titration technique (GITT) (Figure 3A). The galvanostatic potential curve in the in situ cell is almost identical to that for the tests carried out in coin cells (Figure 1B), with both a potential plateau and a sloping potential area, indicative of the diffusion-limited and the non-diffusion-limited regions of the electrochemical lithiation reaction, respectively.

The interlayer distance (c-lattice parameter) can be monitored by the position of the (001) peak, which is at 15.56° 2θ in pristine TiS_2, corresponding to an interlayer distance of 0.569 nm. The initial lithium intercalation up to a composition of about $Li_{0.4}TiS_2$ causes an increase in interlayer spacing (Figure 3B,C), shown by a shift of the (001) peak to

https://doi.org/10.1021/acsenergylett.1c01934
ACS Energy Lett. 2021, 6, 4173−4178

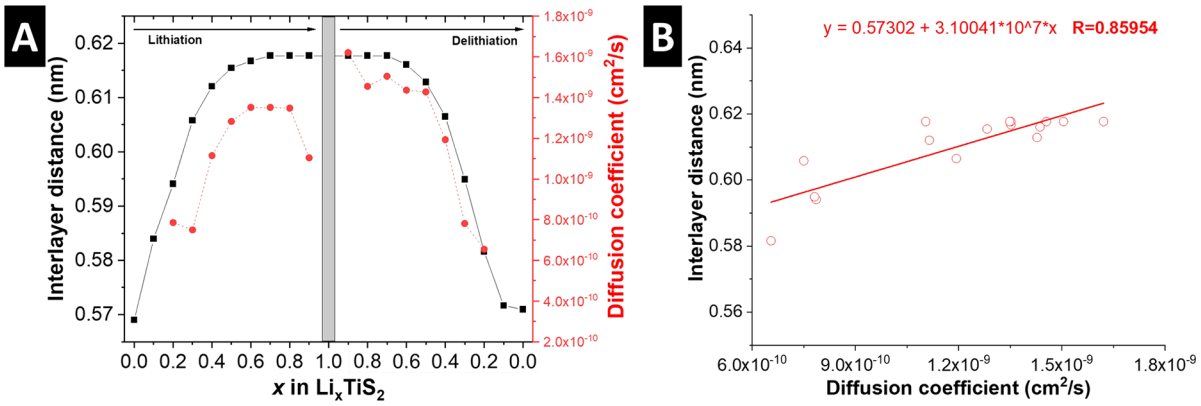

Figure 4. (A) TiS_2 interlayer distance from in situ XRD and Li^+ diffusion coefficient calculated from GITT as a function of Li_xTiS_2 composition during electrochemical lithiation and delithiation. (B) Linear fit of interlayer distance and diffusion coefficient demonstrating positive correlation.

14.46° 2θ (0.612 nm). This region of volumetric expansion corresponds to the diffusion-limited region with a potential plateau in the galvanostatic curve, or a peak in the CV (region I, Figure 3D, where the composition x in Li_xTiS_2 is indicated in the CV based on the integrated charge). Upon further lithiation up to approximately Li_1TiS_2, the interlayer spacing remains almost constant (14.33° 2θ or 0.618 nm), and lithium intercalation occurs practically without further volumetric changes (Figure 3B,C). This region corresponds to the non-diffusion-limited region with a sloping galvanostatic curve, or a rectangular region in the CV (region II). During the delithiation step, the same behavior is mirrored.

Using the GITT data, Li^+ diffusion can be quantified based on Fick's second law.[29] The apparent Li^+ diffusion coefficient D_{Li} can be calculated via

$$D_{Li} = \frac{4}{\pi\tau}\left(\frac{mV_m}{MA}\right)^2\left(\frac{\Delta E_s}{\Delta E_\tau}\right)^2 \quad (2)$$

where τ is the current pulse time (30 min), m is the active material mass, M is the molar mass, V_m is the molar volume, A is the contact area of the active material and electrolyte (defined as the geometrical area of the electrode[30]), ΔE_s is the potential difference between the starting potential and the equilibrium potential (after resting), and ΔE_τ is the potential difference between the starting potential and the potential after the current pulse (before resting).[29] Figure 4A shows interlayer distance and Li^+ diffusion coefficient as a function of Li_xTiS_2 composition. It can clearly be seen that the Li^+ diffusion coefficient increases with growing interlayer distance, up to a composition of about $Li_{0.4}TiS_2$, and then remains constant up to the fully lithiated $LiTiS_2$, at the same time as the interlayer distance remains constant. The equivalent behavior is observed during the electrochemical delithiation process. This strongly indicates that Li^+ transport kinetics correlate with the interlayer spacing in TiS_2, where a larger interlayer spacing results in faster ionic transport (Figure 4B). Such behavior has been theoretically predicted by first-principles simulation.[31] The findings give valuable guidance for the design of high-power intercalation hosts, such as interlayer-functionalized materials with increased interlayer spacing.[32,33]

Based on these observations, a clear link between the electrochemical intercalation kinetics and the electrochemically induced deformation behavior can be made. The kinetics of the lithiation reaction are diffusion-limited when the host material expands/contracts, i.e., undergoes deformation, and they become more and more non-diffusion-limited (pseudocapacitive) when the interlayer is expanded and no more volumetric changes occur in the host material lattice.

The presented study on bulk TiS_2—a model material that exhibits both diffusion- and non-diffusion-limited lithiation regimes—provides some of the most compelling experimental evidence of the intimate relationship between deformation, interlayer distance, and intercalation kinetics.[22] Future work should include analyzing the electro-chemo-mechanical response of electrochemical TiS_2 lithiation on a microscopic level, for example, by using operando atomic force microscopy,[34] including probing of the dynamic response and deformation rate during lithium (de)intercalation.

■ ASSOCIATED CONTENT

Supporting Information

The Supporting Information is available free of charge at https://pubs.acs.org/doi/10.1021/acsenergylett.1c01934.

Experimental details, scanning electron microscopy, XRD, and supplemental electrochemical characterization (CV, *b*-value analysis, EIS) (PDF)

■ AUTHOR INFORMATION

Corresponding Author

Simon Fleischmann − *Université Paul Sabatier, CIRIMAT, 31062 Toulouse, France; Réseau sur le Stockage Electrochimique de l'Energie (RS2E), 80039 Amiens, France;* Present Address: Helmholtz Institute Ulm (HIU), 89081 Ulm, Germany; orcid.org/0000-0001-9475-3692; Email: fleischmann@chimie.ups-tlse.fr

Authors

Hui Shao − *Université Paul Sabatier, CIRIMAT, 31062 Toulouse, France; Réseau sur le Stockage Electrochimique de l'Energie (RS2E), 80039 Amiens, France*

Pierre-Louis Taberna − *Université Paul Sabatier, CIRIMAT, 31062 Toulouse, France; Réseau sur le Stockage Electrochimique de l'Energie (RS2E), 80039 Amiens, France*

Patrick Rozier − *Université Paul Sabatier, CIRIMAT, 31062 Toulouse, France; Réseau sur le Stockage Electrochimique de l'Energie (RS2E), 80039 Amiens, France*

Patrice Simon − *Université Paul Sabatier, CIRIMAT, 31062 Toulouse, France; Réseau sur le Stockage Electrochimique de*

https://doi.org/10.1021/acsenergylett.1c01934
ACS Energy Lett. 2021, 6, 4173−4178

l'Energie (RS2E), 80039 Amiens, France; orcid.org/0000-0002-0461-8268

Complete contact information is available at: https://pubs.acs.org/10.1021/acsenergylett.1c01934

Notes

The authors declare no competing financial interest.

■ ACKNOWLEDGMENTS

S.F. and P.S. acknowledge support from the Agence Nationale de la Recherche (Labex STORE-EX). P.S. was funded by the ERC Synergy Grant MoMa-Stor #951513. The authors thank Dr. Justine Harmel for support with scanning electron microscopy and Barbara Daffos for gas sorption measurements.

■ REFERENCES

(1) Whittingham, M. S. Electrical Energy Storage and Intercalation Chemistry. *Science* **1976**, *192*, 1126−1127.
(2) Whittingham, M. S. Ultimate Limits to Intercalation Reactions for Lithium Batteries. *Chem. Rev.* **2014**, *114*, 11414−11443.
(3) Winter, M.; Barnett, B.; Xu, K. Before Li Ion Batteries. *Chem. Rev.* **2018**, *118*, 11433−11456.
(4) Srimuk, P.; Kaasik, F.; Krüner, B.; Tolosa, A.; Fleischmann, S.; Jäckel, N.; Tekeli, M. C.; Aslan, M.; Suss, M. E.; Presser, V. MXene as a Novel Intercalation-Type Pseudocapacitive Cathode and Anode for Capacitive Deionization. *J. Mater. Chem. A* **2016**, *4*, 18265−18271.
(5) Srimuk, P.; Su, X.; Yoon, J.; Aurbach, D.; Presser, V. Charge-Transfer Materials for Electrochemical Water Desalination, Ion Separation and the Recovery of Elements. *Nat. Rev. Mater.* **2020**, *5*, 517−538.
(6) Liu, C.; Li, Y.; Lin, D.; Hsu, P.-C.; Liu, B.; Yan, G.; Wu, T.; Cui, Y.; Chu, S. Lithium Extraction from Seawater through Pulsed Electrochemical Intercalation. *Joule* **2020**, *4*, 1459−1469.
(7) Yazami, R.; Touzain, P. A Reversible Graphite-Lithium Electrochemical Generators. *J. Power Sources* **1983**, *9*, 365−371.
(8) Li, Y.; Lu, Y.; Adelhelm, P.; Titirici, M. M.; Hu, Y. S. Intercalation Chemistry of Graphite: Alkali Metal Ions and Beyond. *Chem. Soc. Rev.* **2019**, *48*, 4655−4687.
(9) Padhi, A. K.; Nanjundaswamy, K. S.; Goodenough, J. B. Phospho-Olivines as Positive-Electrode Materials for Rechargeable Lithium Batteries. *J. Electrochem. Soc.* **1997**, *144*, 1188−1194.
(10) Meethong, N.; Huang, H. Y. S.; Speakman, S. A.; Carter, W. C.; Chiang, Y. M. Strain Accommodation during Phase Transformations in Olivine-Based Cathodes as a Materials Selection Criterion for High-Power Rechargeable Batteries. *Adv. Funct. Mater.* **2007**, *17*, 1115−1123.
(11) Ohzuku, T.; Ueda, A.; Yamamoto, N. Zero-Strain Insertion Material of Li[Li1/3Ti5/3]O4 for Rechargeable Lithium Cells. *J. Electrochem. Soc.* **1995**, *142*, 1431−1435.
(12) Whittingham, M. S.; Chianelli, R. R. Layered Compounds and Intercalation Chemistry: An Example of Chemistry and Diffusion in Solids. *J. Chem. Educ.* **1980**, *57*, 569−574.
(13) Conway, B. E. Two-Dimensional and Quasi-Two-Dimensional Isotherms for Li Intercalation and UPD Processes at Surfaces. *Electrochim. Acta* **1993**, *38*, 1249−1258.
(14) Fleischmann, S.; Mitchell, J. B.; Wang, R.; Zhan, C.; Jiang, D. E.; Presser, V.; Augustyn, V. Pseudocapacitance: From Fundamental Understanding to High Power Energy Storage Materials. *Chem. Rev.* **2020**, *120*, 6738−6782.
(15) Augustyn, V.; Come, J.; Lowe, M. A.; Kim, J. W.; Taberna, P. L.; Tolbert, S. H.; Abruña, H. D.; Simon, P.; Dunn, B. High-Rate Electrochemical Energy Storage through Li+ Intercalation Pseudocapacitance. *Nat. Mater.* **2013**, *12*, 518−522.
(16) Okubo, M.; Hosono, E.; Kim, J.; Enomoto, M.; Kojima, N.; Kudo, T.; Zhou, H.; Honma, I. Nanosize Effect on High-Rate Li-Ion Intercalation in LiCoO2 Electrode. *J. Am. Chem. Soc.* **2007**, *129*, 7444−7452.
(17) Choi, C.; Ashby, D. S.; Butts, D. M.; DeBlock, R. H.; Wei, Q.; Lau, J.; Dunn, B. Achieving High Energy Density and High Power Density with Pseudocapacitive Materials. *Nat. Rev. Mater.* **2020**, *5*, 5−19.
(18) Muller, G. A.; Cook, J. B.; Kim, H. S.; Tolbert, S. H.; Dunn, B. High Performance Pseudocapacitor Based on 2D Layered Metal Chalcogenide Nanocrystals. *Nano Lett.* **2015**, *15*, 1911−1917.
(19) Cook, J. B.; Lin, T. C.; Kim, H.-S.; Siordia, A.; Dunn, B. S.; Tolbert, S. H. Suppression of Electrochemically Driven Phase Transitions in Nanostructured MoS2 Pseudocapacitors Probed Using Operando X-Ray Diffraction. *ACS Nano* **2019**, *13*, 1223−1231.
(20) Griffith, K. J.; Wiaderek, K. M.; Cibin, G.; Marbella, L. E.; Grey, C. P. Niobium Tungsten Oxides for High-Rate Lithium-Ion Energy Storage. *Nature* **2018**, *559*, 556−563.
(21) Mitchell, J. B.; Geise, N. R.; Paterson, A. R.; Osti, N. C.; Sun, Y.; Fleischmann, S.; Zhang, R.; Madsen, L. A.; Toney, M. F.; Jiang, D. E.; Kolesnikov, A. I.; Mamontov, E.; Augustyn, V. Confined Interlayer Water Promotes Structural Stability for High-Rate Electrochemical Proton Intercalation in Tungsten Oxide Hydrates. *ACS Energy Lett.* **2019**, *4*, 2805−2812.
(22) Augustyn, V.; Wang, R.; Balke, N.; Pharr, M.; Arnold, C. B. Deformation during Electrosorption and Insertion-Type Charge Storage: Origins, Characterization, and Design of Materials for High Power. *ACS Energy Lett.* **2020**, *5*, 3548−3559.
(23) Brunauer, S.; Emmett, P. H.; Teller, E. Adsorption of Gases in Multimolecular Layers. *J. Am. Chem. Soc.* **1938**, *60*, 309−319.
(24) Kasai, H.; Tolborg, K.; Sist, M.; Zhang, J.; Hathwar, V. R.; Filsø, M. Ø.; Cenedese, S.; Sugimoto, K.; Overgaard, J.; Nishibori, E.; Iversen, B. B. X-Ray Electron Density Investigation of Chemical Bonding in van Der Waals Materials. *Nat. Mater.* **2018**, *17*, 249−253.
(25) Thompson, A. H. Lithium Ordering in LixTiS2. *Phys. Rev. Lett.* **1978**, *40*, 1511−1514.
(26) Wang, J.; Polleux, J.; Lim, J.; Dunn, B. Pseudocapacitive Contributions to Electrochemical Energy Storage in TiO2 (Anatase) Nanoparticles. *J. Phys. Chem. C* **2007**, *111*, 14925−14931.
(27) Ko, J. S.; Sassin, M. B.; Rolison, D. R.; Long, J. W. Deconvolving Double-Layer, Pseudocapacitance, and Battery-like Charge-Storage Mechanisms in Nanoscale LiMn2O4 at 3D Carbon Architectures. *Electrochim. Acta* **2018**, *275*, 225−235.
(28) Ko, J. S.; Lai, C.-H.; Long, J. W.; Rolison, D. R.; Dunn, B.; Nelson Weker, J. Differentiating Double-Layer, Psuedocapacitance, and Battery-like Mechanisms by Analyzing Impedance Measurements in Three Dimensions. *ACS Appl. Mater. Interfaces* **2020**, *12*, 14071−14078.
(29) Lim, E.; Shim, H.; Fleischmann, S.; Presser, V. Fast and Stable Lithium-Ion Storage Kinetics of Anatase Titanium Dioxide/Carbon Onion Hybrid Electrodes. *J. Mater. Chem. A* **2018**, *6*, 9480−9488.
(30) Dees, D. W.; Kawauchi, S.; Abraham, D. P.; Prakash, J. Analysis of the Galvanostatic Intermittent Titration Technique (GITT) as Applied to a Lithium-Ion Porous Electrode. *J. Power Sources* **2009**, *189*, 263−268.
(31) Van Der Ven, A.; Thomas, J. C.; Xu, Q.; Swoboda, B.; Morgan, D. Nondilute Diffusion from First Principles: Li Diffusion in LixTiS2. *Phys. Rev. B: Condens. Matter Mater. Phys.* **2008**, *78*, 104306.
(32) Liang, K.; Matsumoto, R. A.; Zhao, W.; Osti, N. C.; Popov, I.; Thapaliya, B. P.; Fleischmann, S.; Misra, S.; Prenger, K.; Tyagi, M.; Mamontov, E.; Augustyn, V.; Unocic, R. R.; Sokolov, A. P.; Dai, S.; Cummings, P. T.; Naguib, M. Engineering the Interlayer Spacing by Pre-Intercalation for High Performance Supercapacitor MXene Electrodes in Room Temperature Ionic Liquid. *Adv. Funct. Mater.* **2021**, *31*, 2104007.
(33) Fleischmann, S.; Spencer, M. A.; Augustyn, V. Electrochemical Reactivity under Confinement Enabled by Molecularly Pillared 2D and Layered Materials. *Chem. Mater.* **2020**, *32*, 3325−3334.
(34) Tsai, W.-Y.; Wang, R.; Boyd, S.; Augustyn, V.; Balke, N. Probing Local Electrochemistry via Mechanical Cyclic Voltammetry Curves. *Nano Energy* **2021**, *81*, 105592.